Perovskite decomposition and missing crystal planes in HRTEM

https://doi.org/10.1038/s41586-021-03423-4

Received: 20 July 2020

Accepted: 4 March 2021

Published online: 9 June 2021

Check for updates

Yu-Hao Deng[1]✉

ARISING FROM Ning, Z. et al. *Nature* https://www.nature.com/articles/nature14563 (2015).

Organic–inorganic hybrid perovskites have recently emerged as a new class of semiconductor for high-performance optoelectronic devices, but their extreme sensitivity to electron beam irradiation hinders our ability to obtain the intrinsic structures from high-resolution transmission electron microscopy (HRTEM) characterizations. Ning and co-workers[1] reported lead sulfide (PbS) quantum dots in methylammonium lead iodide ($MAPbI_3$) solids with perfect lattice matching, on the basis of confirmation from HRTEM, electron diffraction and other studies[1]. However, I have found that some crystal planes were missing in their characterizations, and as demonstrated below, the material in their figures cannot be $MAPbI_3$, but possibly lead iodide (PbI_2)—the product of perovskite decomposed by electron-beam irradiation. This finding aims to raise awareness among researchers and avoid possible mistakes in the HRTEM characterization of electron-beam-sensitive materials in the future.

It is noteworthy that only the $(2\bar{2}4)$, (224) crystal planes appear, and that the $(1\bar{1}2)$, (112) crystal planes are missing in HRTEM characterizations in the original paper[1]. Figure 1a shows the structure of $MAPbI_3$ and Fig. 1b shows the simulated electron diffraction along the $[\bar{2}01]$ zone axis. Clearly, $(1\bar{1}2)$, (112) planes exist in the electron diffraction pattern. Moreover, $(1\bar{1}2)$, (112) planes are also present in HRTEM images under low electron dose[2], selected-area electron diffraction (SAED)[3,4] and X-ray diffraction (XRD)[5–7] characterizations. Figure 1c gives the structure of PbS and Fig. 1d shows the simulated electron diffraction along the $[11\bar{1}]$ zone axis. Unlike the *I*4/*mcm* space group of tetragonal $MAPbI_3$, the $Fm\bar{3}m$ space group of cubic PbS displays systematic extinction[8], so there should be no {101} planes visible in the electron diffraction pattern of PbS phase[9].

$MAPbI_3$ perovskite is very sensitive to electron-beam irradiation and begins to decompose into PbI_2 under 151 e Å^{-2} total dose irradiation[10] (e, electron charge). The absence of crystal planes indicates that the material is no longer $MAPbI_3$ perovskite, but other phases and structures[10–12]. Figure 1e shows the structure of PbI_2 and Fig. 1f shows the electron diffraction pattern along the $[8\bar{8}1]$ axis zone, which is consistent with the parameters in the original paper. Importantly, the angle between $(2\bar{2}4)$ and (224) is about 57°, not 60° under exact measurement in the

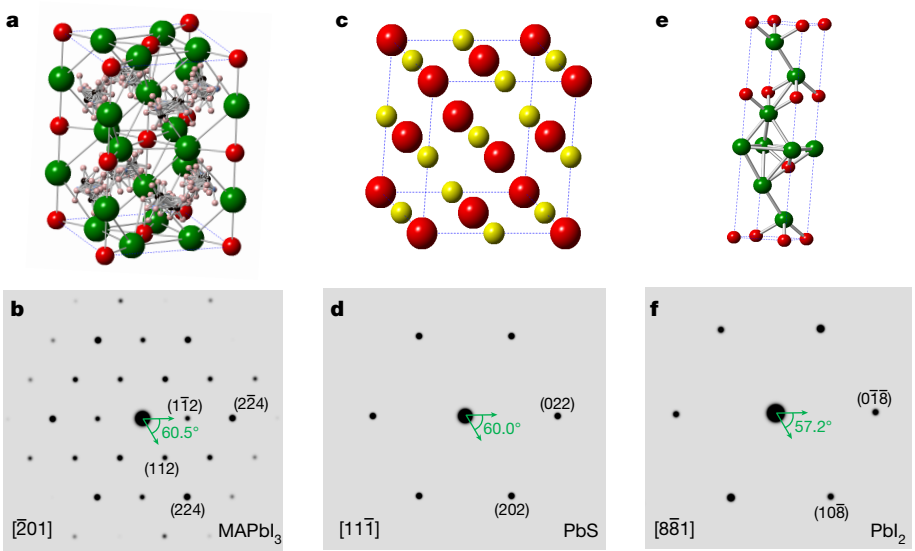

Fig. 1 | Ball and stick models, simulated electron diffraction patterns of $MAPbI_3$, PbS and PbI_2. a, The atomic ball and stick model of $MAPbI_3$. **b**, The simulated electron diffraction pattern of $MAPbI_3$. **c**, The structure of PbS. **d**, The simulated electron diffraction pattern of PbS. The $(1\bar{1}2)$, (112) planes appear in $MAPbI_3$ because of the *I*4/*mcm* space group. However, there are no {101} planes displayed in the electron diffraction pattern of cubic PbS phase ($Fm\bar{3}m$ space group) due to systematic extinction. **e**, The structure of PbI_2. **f**, The electron diffraction pattern of PbI_2. The distances and angles between crystal planes in electron diffraction pattern of PbI_2 are very similar to parameters in the original paper. Here, colours represent the following: red, lead; green, iodine; pink-blue group, methylamine; yellow, sulfur.

[1]Department of Chemistry, Ghent University, Ghent, Belgium. ✉e-mail: yuhaodeng@pku.edu.cn

Table 1 | Detailed parameters in the original paper, PbS, $MAPbI_3$ and PbI_2

Material	Crystal structure	Space group	Cell parameters	Characteristic lattice planes	Interplanar spacing	Interplanar angle
$MAPbI_3$ in Ning et al.[1]				$(2\bar{2}4)$, (224)	$d(2\bar{2}4) = d(224) = 2.2$ Å	$\langle(2\bar{2}4), (224)\rangle = 57.4°$
PbS in Ning et al.[1]				(022), (202)	$d(022) = d(202) = 2.1$ Å	$\langle(022), (202)\rangle = 57.5°$
$MAPbI_3$	Tetragonal	$I4/mcm$	$a = b = 8.839$ Å, $c = 12.695$ Å	$(1\bar{1}2)$, (112)	$d(1\bar{1}2) = d(112) = 4.44$ Å	$\langle(1\bar{1}2), (112)\rangle = \langle(2\bar{2}4), (224)\rangle = 60.5°$
			$\alpha = \beta = \gamma = 90°$	$(2\bar{2}4)$, (224)	$d(2\bar{2}4) = d(224) = 2.22$ Å	
PbS	Cubic	$Fm\bar{3}m$	$a = b = c = 5.929$ Å	(022), (202)	$d(022) = d(202) = 2.10$ Å	$\langle(022), (202)\rangle = 60.0°$
			$\alpha = \beta = \gamma = 90°$			
PbI_2	Hexagonal	$P\bar{3}m1$	$a = b = 4.555$ Å, $c = 20.937$ Å	$(0\bar{1}\bar{8})$, $(10\bar{8})$	$(0\bar{1}\bar{8}) = d(10\bar{8}) = 2.18$ Å	$\langle(0\bar{1}\bar{8}), (10\bar{8})\rangle = 57.2°$
			$\alpha = \beta = 90°$, $\gamma = 120°$			

Angled brackets (⟨ and ⟩) represent the angle between two crystal planes.

original paper. To make the comparison clearer, Table 1 shows the detailed parameters from the original paper[1] and for PbS, $MAPbI_3$ and PbI_2.

In light of above clarification, the structure in the HRTEM images of the original paper[1] is more likely to be PbI_2, and the higher-contrast spots are caused by the mass thickness contrast effect[13]. Owing to lack of the corresponding in situ high-angle annular dark-field scanning transmission electron microscopy (HAADF-STEM) image in the original paper, it is impossible to prove that the higher-contrast spots are PbS quantum dots rather than PbI_2 particles. Next, the authors should check the experimental conditions of HRTEM, especially the dose of the electron-beam irradiation. If possible, it would also be better if they compared the particle size and size distribution of colloidal quantum dots and quantum dots in perovskite in the original paper. Moreover, a low dose[10–15] and low temperature[2,13] can reduce the damage of electron-beam irradiation to perovskite, and may help to obtain the real structure of the quantum dots in perovskite solids.

Methods

The electron diffraction simulations of $MAPbI_3$, PbS and PbI_2 were obtained using CrystalMaker Software. Corresponding CIF files of their crystal structures were downloaded from the Crystallography Open Database (COD) (http://www.crystallography.net/cod). The COD IDs of $MAPbI_3$, PbS and PbI_2 are 4124388, 5000087 and 9009141, respectively. $MAPbI_3$ is a $I4/mcm$ space group with tetragonal structure, cell parameters: $a = b = 8.839$ Å, $c = 12.695$ Å and $\alpha = \beta = \gamma = 90°$. PbS is an $Fm\bar{3}m$ space group with cubic structure, cell parameters: $a = b = c = 5.929$ Å and $\alpha = \beta = \gamma = 90°$. PbI_2 is a $P\bar{3}m1$ space group with hexagonal structure, cell parameters: $a = b = 4.555$ Å, $c = 20.937$ Å and $\alpha = \beta = 90°$, $\gamma = 120°$. It is important to note that PbI_2 has many possible polytypes. During the process of phase identification, I also tried other polytypes of PbI_2, but the results did not match well with the original paper data.

Data availability

All data are available from the corresponding author upon reasonable request.

1. Ning, Z. et al. Quantum-dot-in-perovskite solids. *Nature* **523**, 324–328 (2015).
2. Zhu, Y. et al. Direct atomic scale characterization of the surface structure and planar defects in the organic-inorganic hybrid $CH_3NH_3PbI_3$ by cryo-TEM. *Nano Energy* **73**, 104820 (2020).
3. Pham, H. T. et al. Insights into twinning formation in cubic and tetragonal multi-cation mixed-halide perovskite. *ACS. Mater. Lett.* **2**, 415–424 (2020).
4. Rothmann, M. U. et al. Direct observation of intrinsic twin domains in tetragonal $CH_3NH_3PbI_3$. *Nat. Commun.* **8**, 14547 (2017).
5. Ding, J. et al. A self-powered photodetector based on a $CH_3NH_3PbI_3$ single crystal with asymmetric electrodes. *Cryst. Eng. Comm.* **18**, 4405–4411 (2016).
6. Dong, Q. et al. Electron-hole diffusion lengths >175 μm in solution-grown $CH_3NH_3PbI_3$ single crystals. *Science* **347**, 967–970 (2015).
7. Zhang, X. W. et al. Directly imaging the structure–property correlation of perovskites in crystalline microwires. *J. Mater. Chem. A* **7**, 13305–13314 (2019).
8. Hammond, C. *The Basics of Crystallography and Diffraction* (Oxford Univ. Press, 2001).
9. Fu, X. et al. Quantum confinement effects on charge-transfer between PbS quantum dots and 4-mercaptopyridine. *J. Chem. Phys.* **134**, 024707 (2011).
10. Chen, S. et al. Atomic scale insights into structure instability and decomposition pathway of methylammonium lead iodide perovskite. *Nat. Commun.* **9**, 4807 (2018).
11. Rothmann, M. U. et al. Microstructural characterisations of perovskite solar cells—from grains to interfaces: techniques, features, and challenges. *Adv. Energy Mater.* **7**, 1700912 (2017).
12. Deng, Y. H. & Nest, L. G. Analysis of misidentifications in TEM characterization of organic–inorganic hybrid perovskite material. *J. Microsc.* https://doi.org/10.1111/jmi.13000 (2021).
13. Li, Y. et al. Unravelling degradation mechanisms and atomic structure of organic–inorganic halide perovskites by cryo-EM. *Joule* **3**, 2854–2866 (2019).
14. Zhang, D. et al. Atomic-resolution transmission electron microscopy of electron beam–sensitive crystalline materials. *Science* **359**, 675–679 (2018).
15. Rothmann, M. U. et al. Atomic-scale microstructure of metal halide perovskite. *Science* **370**, eabb5940 (2020).

Acknowledgements I thank the original authors for discussions and anonymous reviewers for suggestions. I also appreciate encouragement from Y. Xiong. This friendly Matters Arising only aims to perfect the original paper and benefit the development of the academic community.

Author contributions All findings, simulations, data analysis and writing in this paper were undertaken by Y.-H.D.

Competing interests The authors declare no competing interests.

Additional information
Correspondence and requests for materials should be addressed to Y.-H.D.

Reply to: Perovskite decomposition and missing crystal planes in HRTEM

https://doi.org/10.1038/s41586-021-03424-3

Published online: 9 June 2021

Check for updates

Zhijun Ning[1,15], Xiwen Gong[2,3,4,5,6,15], Riccardo Comin[7,15], Grant Walters[8], Fengjia Fan[9,10,11,12], Oleksandr Voznyy[13], Emre Yassitepe[14], Andrei Buin[8], Sjoerd Hoogland[8] & Edward H. Sargent[8]✉

In our Letter published in 2015[1], we reported epitaxial growth of perovskite around PbS quantum dots. The quantum dot surface is passivated by the crystalline perovskite scaffolding without the need of conventional ligands, leading to a two-orders-of-magnitude enhancement in the photoluminescence quantum yield in infrared quantum dot films. This material provided efficient charge carrier transfer from the perovskite to the quantum dots, enabling sensitization.

In the accompanying Comment[2], Deng asks whether there is enough evidence for PbS being embedded into perovskite, and in particular whether TEM images in the original Letter correspond to PbI_2 as opposed to perovskite or PbS. Deng noted a difference in the estimated interplanar angle in his analysis of our published data (Deng finds 57°) compared to the value we report (60°). Deng also points out the absence of a diffraction spot related to the (112) plane of perovskite and suggests possible perovskite degradation.

The coexistence of perovskite and quantum dots is supported in the original Letter[1] by optical absorption spectra, static and transient photoluminescence spectra, photoluminescence excitation spectra, X-ray photoelectron spectroscopy (XPS), high-angle annular dark-field imaging scanning transmission electron microscopy (HAADF-STEM) and Rutherford backscattering spectrometry (RBS). The density functional theory (DFT) simulations show that epitaxial alignment is possible and is needed to avoid interfacial traps.

In light of Deng's questions, we revisited the analysis of the interplanar angle and the missing diffraction spots. Since the fast Fourier transform (FFT) is performed on a small subsection of the image to capture the PbS and perovskite lattices separately, the resulting diffraction pattern is diffused, and this leads to a range in determining the centre of each spot, and consequently to a range in angular estimates. Both pre-2015 and contemporaneous 2015 high-resolution transmission electron microscopy (HRTEM) studies also lacked evidence of the (112) plane reflection[3–9]. We agree that there is a possibility of perovskite degradation to PbI_2 (ref. [3]).

Given this possibility, we sought therefore—in light of advances in transmission electron microscopy (TEM) over the past six years—to investigate the materials using improved TEM equipment (aberration-corrected JEOL GrandARM (ARM300F)). We used the method of sample preparation described in the 2015 Letter[1]. We reduced the electron dose to 10 e Å^{-2} (e, electron charge), and see the characteristic Fourier spots attributed to {110} facets of $MAPbI_3$ (Fig. 1a, b, d).

Since this fourfold symmetry pattern with d = 6.5 Å (±5%) is specific to $MAPbI_3$ and is absent in trigonal PbI_2 (ref. [10]), this indicates that the perovskite crystal structure remains intact.

We performed electron energy loss spectroscopy (EELS) spot-detection elemental analysis in selected areas (dashed boxes in Fig. 1a) and observed the $S_{L2,3}$ edge at 165 eV—evidence of sulfur in the selected area (red box in Fig. 1e). This indicates that PbS quantum dots are embedded in the perovskite matrix. For comparison, we select another area (green box) for EELS, and observed no $S_{L2,3}$ edge (Fig. 1e). We do not observe lattice distortion within the perovskite matrix in the region that contains PbS.

The new HRTEM images and the accompanying elemental analysis, together with optical and electronic properties, XPS and RBS from the original Letter, support the finding of dots in perovskite. The evidence of epitaxial alignment comes from the suite of characterization studies reported in the original work. Specifically, DFT reveals that the interfacial energy between PbS (110) and $MAPbI_3$ (110) is less than 10 meV Å^{-2}, suggesting that the epitaxial growth of perovskite on PbS is as energetically feasible as homoepitaxy of PbS on PbS or perovskite on perovskite. The enhanced photoluminescence quantum efficiency (PLQE) of colloidal quantum dots (CQDs) embedded in perovskite matrix compared to pure CQD or CQD-in-matrix with poor lattice matching is consistent with the formation of epitaxial interfaces. The photoluminescence excitation spectra of the CQD in perovskite matrix and the high transfer efficiency of 80% from perovskite matrix into dots agree with the low defect density at the perovskite-CQD interface.

The use of PbS quantum dots in perovskite has been further investigated by a number of groups. Jung et al. reported using DFT that high-quality heteroepitaxy between PbS (100) and $CsPbBr_3$ (100) was energetically favourable for both materials[11]. Masi et al. demonstrated the role of lattice matching at the heteroepitaxial interface between perovskite shell (MA) and PbS CQDs and its influence on the optoelectronic properties of PbS CQDs. High mobility (1.3 cm^2 V^{-1} s^{-1}) and high detectivity (2×10^{11} cm Hz$^{1/2}$ W^{-1} with >110 kHz bandwidth) was achieved when the lattice constant mismatch is minimized between PbS and the perovskite shell[12]. Zhang et al. reported, on the basis of HRTEM, epitaxial coherence between the $CsPbI_3$ and PbS CQD lattice[13]. Liu et al., using TEM, reported that $CsPbBr_xI_{3-x}$ perovskites inherit the crystalline orientation of the embedded PbS quantum dots[14]. Improved performance has been observed in PbS-dot-in-perovskite solar cells, photodetectors, and light emitting diodes[13,15–17].

[1]School of Physical Science and Technology, ShanghaiTech University, Shanghai, China. [2]Department of Chemical Engineering, University of Michigan, Ann Arbor, MI, USA. [3]Department of Materials Science and Engineering, University of Michigan, Ann Arbor, MI, USA. [4]Department of Electrical Engineering and Computer Science, University of Michigan, Ann Arbor, MI, USA. [5]Macromolecular Science and Engineering Program, University of Michigan, Ann Arbor, MI, USA. [6]Applied Physics Program, University of Michigan, Ann Arbor, MI, USA. [7]Department of Physics, Massachusetts Institute of Technology, Cambridge, MA, USA. [8]Department of Electrical and Computer Engineering, University of Toronto, Toronto, Ontario, Canada. [9]Hefei National Laboratory for Physical Sciences at the Microscale, University of Science and Technology of China, Hefei, China. [10]Department of Modern Physics, University of Science and Technology of China, Hefei, China. [11]CAS Key Laboratory of Microscale Magnetic Resonance, University of Science and Technology of China, Hefei, China. [12]Synergetic Innovation Center of Quantum Information and Quantum Physics, University of Science and Technology of China, Hefei, China. [13]Department of Physical and Environmental Sciences, University of Toronto Scarborough, Scarborough, Ontario, Canada. [14]Department of Physics, University of Maranhão, São Luís, Brazil. [15]These authors contributed equally: Zhijun Ning, Xiwen Gong, Riccardo Comin. ✉e-mail: ted.sargent@utoronto.ca

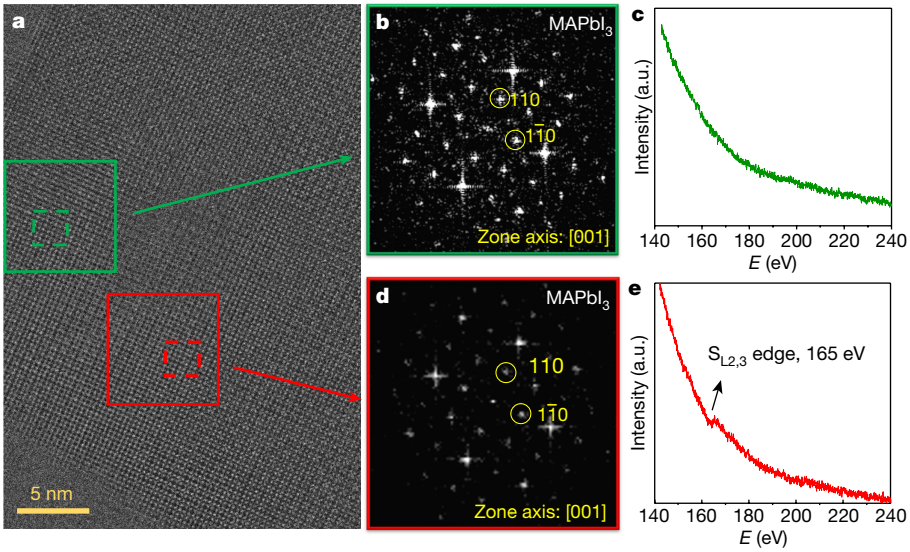

Fig. 1 | TEM analysis of quantum dots in perovskite. a, HRTEM image. The red and green solid boxes denote the regions in which we performed FFT; the red and green dashed boxes represent the regions in which we performed EELS analysis. **b**, FFT image of the green solid box in HRTEM. **c**, The green curve shows the EELS spectrum from the green dashed box in **a**; no edge of sulfur is observed. **d**, FFT image of the red solid box in **a**. **e**, The red curve represents the EELS spectrum acquired from the red dashed box in **a**; the $S_{L2,3}$ edge at 165 eV corresponds to element sulfur, indicating PbS quantum dots. a.u., arbitrary units.

We once again thank Deng for having motivated a fruitful dialogue and updates to the TEM studies of the original paper.

Data availability

The data within this paper and findings of this study are available from the corresponding author upon reasonable request.

1. Ning, Z. et al. Quantum-dot-in-perovskite solids. *Nature* **523**, 324–328 (2015).
2. Deng, Y.-H. Perovskite decomposition and missing crystal planes in HRTEM. *Nature* https://doi.org/10.1038/s41586-021-03423-4 (2021).
3. Chen, S. et al. Atomic scale insights into structure instability and decomposition pathway of methylammonium lead iodide perovskite. *Nat. Commun.* **9**, 4807 (2018).
4. Zhu, H. et al. Lead halide perovskite nanowire lasers with low lasing thresholds and high quality factors. *Nat. Mater.* **14**, 636–642 (2015).
5. Gao, L. et al. Passivated single-crystalline $CH_3NH_3PbI_3$ nanowire photodetector with high detectivity and polarization sensitivity. *Nano Lett.* **16**, 7446–7454 (2016).
6. Kollek, T. et al. Porous and shape-anisotropic single crystals of the semiconductor perovskite $CH_3NH_3PbI_3$ from a single-source precursor. *Angew. Chem. Int. Ed.* **54**, 1341–1346 (2015).
7. Son, D. Y. et al. Self-formed grain boundary healing layer for highly efficient $CH_3NH_3PbI_3$ perovskite solar cells. *Nat. Energy* **1**, 16081 (2016).
8. Long, M. et al. Textured $CH_3NH_3PbI_3$ thin film with enhanced stability for high performance perovskite solar cells. *Nano Energy* **33**, 485–496 (2017).
9. Zhu, F. et al. Shape evolution and single particle luminescence of organometal halide perovskite nanocrystals. *ACS Nano* **9**, 2948–2959 (2015).
10. Fan, Z. et al. Layer-by-layer degradation of methylammonium lead tri-iodide perovskite microplates. *Joule* **1**, 548–562 (2017).
11. Jung, Y. K., Butler, K. T. & Walsh, A. Halide perovskite heteroepitaxy: bond formation and carrier confinement at the PbS–$CsPbBr_3$ interface. *J. Phys. Chem. C* **121**, 27351–27356 (2017).
12. Sytnyk, M. et al. Quasi-epitaxial metal–halide perovskite ligand shells on PbS nanocrystals. *ACS Nano* **11**, 1246–1256 (2017).
13. Zhang, X. et al. Inorganic $CsPbI_3$ perovskite coating on PbS quantum dot for highly efficient and stable infrared light converting solar cells. *Adv. Energy Mater.* **8**, 1702049 (2018).
14. Liu, M. et al. Lattice anchoring stabilizes solution-processed semiconductors. *Nature* **570**, 96–101 (2019).
15. Masi, S. et al. Chemi-structural stabilization of formamidinium lead iodide perovskite by using embedded quantum dots. *ACS Energy Lett.* **5**, 418–427 (2020).
16. Zhang, X. et al. PbS capped $CsPbI_3$ nanocrystals for efficient and stable light-emitting devices using p-i-n structures. *ACS Cent. Sci.* **4**, 1352–1359 (2018).
17. Peng, J., Chen, Y., Zhang, X., Dong, A. & Liang, Z. Solid-state ligand-exchange fabrication of $CH_3NH_3PbI_3$ capped PbS quantum dot solar cells. *Adv. Sci.* **3**, 1500432 (2015).

Acknowledgements The TEM characterization was supported by the Center for High-resolution Electron Microscopy (ChEM) at ShanghaiTech University. We thank Y. Yu, B. Yuan and K. Xu at ShanghaiTech University for the TEM measurement. We thank Y. Li at Stanford University for discussions.

Author contributions X.G., Z.N., O.V. and E.H.S. designed and directed this study. Z.N. led the experimental work. X.G., Z.N., O.V. and E.H.S. wrote the manuscript. R.C., F.F., E.Y. and S.H. participated in discussions. All authors contributed to reviewing and commenting on the manuscript.

Competing interests The authors declare no competing interests.

Additional information
Correspondence and requests for materials should be addressed to E.H.S.
Reprints and permissions information is available at http://www.nature.com/reprints.
Publisher's note Springer Nature remains neutral with regard to jurisdictional claims in published maps and institutional affiliations.